Proton Transfer Reactions Linked to Rhodopsin Activation†

Istvan Szundi,‡ Tina L. Mah,‡,§ James W. Lewis,‡ Stefan Jäger,‡,|| Oliver P. Ernst,⊥ Klaus Peter Hofmann,⊥ and David S. Kliger*,‡

Department of Chemistry and Biochemistry, University of California, Santa Cruz, Santa Cruz, California 95064, and Institut für Medizinische Physik und Biophysik, Charité, Medizinische Fakultät der Humboldt-Universität zu Berlin, Ziegelstrasse 5-9, 10098 Berlin, Germany

Received May 27, 1998; Revised Manuscript Received August 4, 1998

ABSTRACT: Purified bovine rhodopsin solubilized in dodecyl maltoside was photolyzed at 20 °C with 477 nm light, and difference spectra were collected at time delays ranging from 10 μs to 10 ms after photolysis. Bromocresol purple was added to the samples to detect pH changes in the aqueous environment due to changes in the protonation state of rhodopsin. The data were analyzed using singular value decomposition and global exponential fitting, which revealed three exponential processes indicating the presence of at least four intermediates. Spectral changes of the indicator dye were separated from those of rhodopsin, and proton release and uptake rates were analyzed within the framework of rhodopsin photoreaction kinetics. Proton release occurred during Lumi decay to Meta-I_{380} followed by uptake upon Meta-I_{380} decay and by a more significant proton uptake with the time course of Meta-I_{480} decay. On the basis of the estimated number of protons released and taken up in each step of the rhodopsin photoreaction, we concluded that two forms of Meta-II are present. The two forms of Meta-II, Meta-$II_{a'}$ and Meta-II_b, differ in protonation state from one another as do both from the earlier, 380 nm absorbing form, Meta-I_{380}.

The heptahelical transmembrane protein rhodopsin is a visual pigment whose activation after absorption of visible light is initiated by a cis to trans isomerization of its 11-*cis*-retinal chromophore. As the protein relaxes, it undergoes a series of chromophore and protein conformational changes that can be detected by associated spectral changes. The scheme for the late intermediates shown below was proposed by Thorgeirsson et al. (*1*) on the basis of kinetic absorption measurements:

Scheme 1

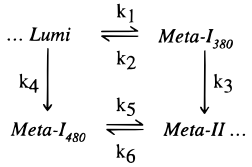

Lumirhodopsin (Lumi),[1] the first intermediate observed on the microsecond time scale at room temperature, decays through several forms of metarhodopsin (Meta) in the process of reaching the active form of the photoreceptor protein. The scheme includes Meta-I_{380}, an early intermediate with a deprotonated retinylidene Schiff base, absorbing at 380 nm, which is kinetically distinct from the classical Meta-II intermediate. Since it is an early metarhodopsin intermediate, it is designated as Meta-I_{380} (with the conventional Meta-I designated by Meta-I_{480}). Meta-II, originally characterized by Matthews et al. (*2*), also has a deprotonated Schiff base linkage and is known to assume a conformation in which it can interact with transducin (*3*) to initiate a cascade of biochemical reactions resulting in visual transduction.

Besides Meta-I_{380} and Meta-II, other isochromic intermediates with absorption maxima at 380 nm have been proposed. On the basis of proton uptake measurements, Arnis and Hofmann (*4*) derived the following scheme for the late intermediates:

Scheme 2

$$\ldots \text{Meta-I} \rightleftharpoons \text{Meta-II}_a \overset{+H^+}{\rightleftharpoons} \text{Meta-II}_b \ldots$$

Meta-II_a corresponds to a conformational state in which the Schiff base proton has translocated to another internal group within the protein, and Meta-II_b corresponds to a conformational state resulting in spectrally silent net proton uptake from the aqueous phase. In the presence of the G-protein, G_t, photoregeneration back to the initial state is blocked under conditions of Meta-II_b (but not Meta II_a) formation, which led Arnis and Hofmann (*5*) to the conclusion that the Meta-II_b is the one that binds G_t. The sequential Meta-II_a/Meta-II_b scheme does not exclude more complex reaction schemes, including an inhomogeneous Meta-II_a state (*4*).

Since the two schemes, each containing two deprotonated Schiff base intermediates, were derived from different types of experimental data, it is of interest to explore the relation-

† This work was supported by Grant EY00983 (to D.S.K.) from the National Eye Institute of the National Institutes of Health and by the Deutsche Forschungsgemeinschaft (SFB 366, to K.P.H.).

‡ University of California, Santa Cruz.

§ Present address: Department of Geology & Geophysics, University of California, Berkeley, Berkeley, CA 94720.

|| Present address: Evotec BioSystems GmbH, Schnackenburgallee 114, 22525 Hamburg, Germany.

⊥ Humboldt-Universität zu Berlin.

[1] Abbreviations: bcp, bromocresol purple; Lumi, lumirhodopsin; MES, 2-(*N*-morpholino)ethanesulfonic acid; Meta, metarhodopsin; rho, rhodopsin.

S0006-2960(98)01249-5 CCC: $15.00
Published on Web 09/16/1998

ships between these intermediates. This could help decipher whether Schiff base deprotonation and proton uptake occur in one concerted reaction (*2*, *6*) or whether they occur in two steps as suggested by Arnis and Hofmann (*4*). Simultaneous observation of Meta-I_{380} and the two forms of Meta-II is difficult in membrane suspensions because Meta-I_{480} competes with Meta-I_{380} as a precursor to Meta-II (*7*). However, in detergent Meta-I_{380} becomes the predominant precursor to Meta-II allowing all three 380 nm absorbing forms to be characterized. Understanding of intermediates in detergent solutions has become more important since transducin activation by rhodopsin mutants is often assayed in dodecyl maltoside and differences have been observed between detergent and membrane preparations (*8*). Also, in detergents Meta-II_a and Meta-II_b can be resolved kinetically, allowing their relationship to Meta-I_{380} to be determined. The aim of this study is to obtain a better understanding of the reaction steps involved in the interconversions between rhodopsin late intermediates leading to transducin activation and to gain insight into the relationships between the isospectral intermediates of the two schemes by detecting proton uptake and release using indicator dye.

EXPERIMENTAL PROCEDURES

Sample Preparation. Disk membranes were isolated from bovine rod outer segments, and the rhodopsin was purified by affinity chromatography on concanavalin A columns as described previously (*9*). After elution the rhodopsin sample was dialyzed against a solution containing 130 mM NaCl and 0.6 mM dodecyl maltoside. For the experiments conducted here, three types of samples were prepared: one with 50 μM bromocresol purple (bcp) to detect proton uptake and release (called rho/bcp), one with 50 μM bromocresol purple and 50 mM 2-(*N*-morpholino)ethanesulfonic acid (MES) as a buffer (called rho/bcp/MES), and one with neither dye nor buffer for control purposes (called rho). All samples contained 0.24 mg/mL rhodopsin, 1.2 mM dodecyl maltoside (an average of two micelles per rhodopsin), and 155 mM NaCl. The pH was adjusted to 6.3 before each experiment and checked for stability over the course of the experiment.

Calibration of pH Indicator. Bromocresol purple absorbs at about 425 nm in its acidic form and at about 590 nm in its basic form. A spectroscopic titration was performed by measuring spectra of room-temperature rho/bcp samples before and after addition of 2 μM HCl or NaOH. The spectral change induced by a 2 μM proton difference was used to calibrate pH changes observed in time-resolved spectral measurements.

Photolysis Experiments. The third harmonic of a Nd:YAG laser was used to pump a dye laser that photolyzed the sample with pulses of 477 nm light (7 ns fwhm, 0.65 mJ/pulse/10 mm^2 area). The probe beam, provided by a xenon short arc flashlamp (*10*, *11*), entered the sample at an angle of 90° from the laser beam. Transmitted probe light was detected using an optical multichannel analyzer described previously (*10*). Absorption difference spectra were collected at time delays ranging from 10 μs to 10 ms after photolysis. A temperature-controlled sample cell was employed to maintain the sample at 20 °C. Further details about the apparatus are described elsewhere (*12*).

Data Analysis. Singular value decomposition was utilized to reduce the number of parameters which needed to be determined by the least-squares global analysis procedure used to fit the data to a series of exponential functions. These methods are explained in detail elsewhere (*13*−*15*).

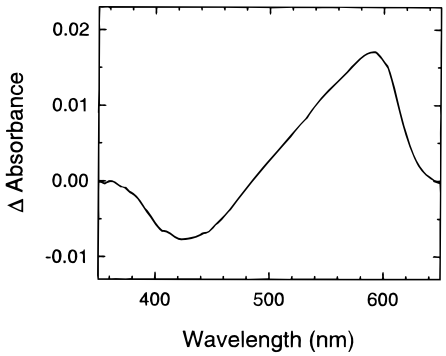

FIGURE 1: Difference spectrum produced by addition of 2 μM NaOH to a purified rhodopsin sample (initially at pH 6.3) containing 50 μM bromocresol purple at room temperature.

To use the results of the global exponential fit to test a model such as Scheme 1, the conversions between the intermediates are expressed as

$$\frac{d\mathbf{c}}{dt} = \mathbf{K}\mathbf{c} \tag{1}$$

where **c** is a vector whose components are the concentrations of the intermediates and **K**, the kinetic matrix, contains the microscopic rate constants. The solution to this set of differential equations is

$$\mathbf{c}(t) = \sum_{i=1}^{n} f_i \mathbf{a}_i \exp(\alpha_i t) \tag{2}$$

where n represents the number of intermediates, f_i is a factor that can be determined from the initial intermediate concentrations, $\mathbf{a}_i$ represents the eigenvectors of the kinetic matrix, and α_i represents its eigenvalues.

The eigenvectors are related to the *b*-spectra (amplitudes associated with each apparent rate obtained from global analysis) by the following equation

$$\mathbf{b}_i(\lambda) = \epsilon(\lambda) f_i \mathbf{a}_i \tag{3}$$

where $\mathbf{b}_i(\lambda)$ represents the *b*-spectra and $\epsilon(\lambda)$ represents the intermediate minus bleach spectra. The eigenvalues are the apparent rates. The best fits for a given model can be obtained by altering the microscopic rates in the kinetic matrix as constrained by the apparent rates so that the eigenvectors, combined with realistic intermediate spectra, reproduce the measured *b*-spectra (*1*, *16*). In these studies a sum of asymmetric Gaussians was employed to model the absorption spectra of all species.

Sign Conventions. Positive absorbance near 600 nm in a raw difference spectrum (e.g., Figure 1) indicates that the medium has become more alkaline at the time delay at which that difference spectrum was collected. The same convention is used to interpret the time-independent (b_0) spectrum which represents the spectra of the final products (i.e., a difference spectrum collected at infinite time). The *b*-spectra corresponding to nonzero apparent rates are called the time-dependent *b*-spectra and describe the spectral changes associated with transitions between intermediate states. The

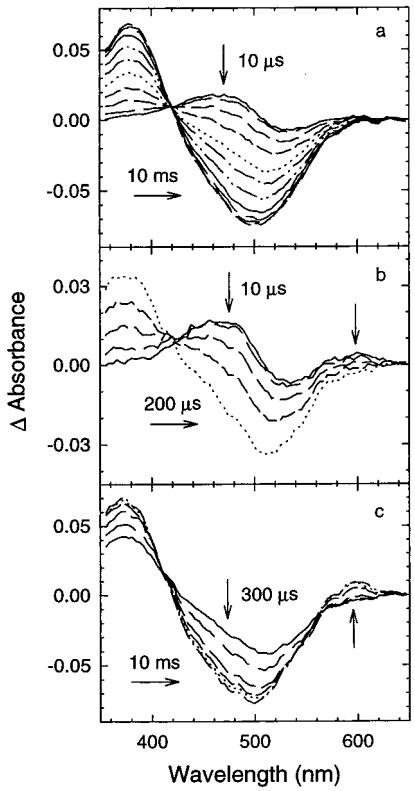

FIGURE 2: Time-resolved absorption difference spectra of purified rhodopsin solubilized in dodecyl maltoside at 20 °C, pH 6.3. Time delays after 477 nm photolysis are 10, 20, 50, 100, 200, 300, and 500 μs and 1, 2, 5, and 10 ms. Arrows show the direction of absorbance changes. (a) Rhodopsin without indicator dye. (b) Rhodopsin with bromocresol purple dye at time delays ranging from 10 μs to 200 μs. (c) Rhodopsin with dye at time delays ranging from 0.3 to 10 ms.

convention used for interpretation of the time-dependent *b*-spectra is different from the one which governs interpretation of raw absorption difference spectra and b_0. Positive absorbance in the time-dependent *b*-spectra is associated with decaying intermediates, and negative absorbance is associated with forming intermediates. Thus a positive absorbance in the 600 nm region would indicate that the medium is becoming more acidic and a negative absorbance would indicate that the medium is becoming more alkaline during the transition represented by that particular *b*-spectrum.

RESULTS

Absorption Difference Spectra. The difference spectrum corresponding to the removal of 2 μM protons for rho/bcp samples is shown in Figure 1. The data indicates that a 2 μM change corresponds to about a 17 mOD absorbance change at 593 nm. Difference spectra for time-resolved experiments of rho and rho/bcp samples appear in Figure 2. Comparison of rho (Figure 2a) with rho/bcp (Figure 2b,c) shows substantial absorbance changes in the 600 nm region from dye spectral changes associated with pH changes. Separation of the data into sets containing early ($\leq$200 μs) and late ($\geq$300 μs) time delays reveals an absorbance decrease from 10 to about 200 μs (Figure 2b) and an absorbance increase from about 1 to 10 ms in the 600 nm region (Figure 2c).

Exponential Fitting and Comparison of rho/bcp and rho b-Spectra. The time dependence of the absorption spectra

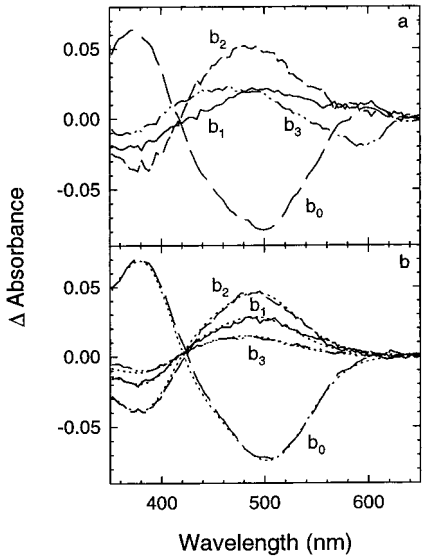

FIGURE 3: Absorbance changes (*b*-spectra) associated with exponential processes observed after photolysis of purified rhodopsin solubilized in dodecyl maltoside at 20 °C, pH 6.3. (a) *b*-Spectra in the presence of indicator dye. (b) *b*-Spectra in the absence of dye and fit of Scheme 1 to *b*-spectra. Each *b*-spectrum has contributions from specific intermediate decay processes as follows: Lumi to Meta-I_{380} (b_1, fast process), the equilibrated mixture of Lumi and Meta-I_{380} to Meta-I_{480} and Meta-II (b_2, middle process), Meta-I_{480} to Meta-II (b_3, slow process). The final spectrum of the equilibrated mixture of Meta-I_{480} and Meta-II minus the spectrum of the bleached rhodopsin determines b_0, the time-independent process. Line types are (—) for b_1, (---) for b_2, (—••—) for b_3, (— — —) for b_0, and (•••) for fits.

for all three sample types showed three exponentials, indicating the presence of a minimum of four intermediates consistent with Scheme 1. The corresponding lifetimes for the three samples were very similar, suggesting that absorption changes due to the progression of rhodopsin photointermediates are dominant. The lack of additional exponentials due to absorption changes of the dye may indicate that the protonation changes parallel the rhodopsin kinetics or that deviation of the dye kinetics from those of the rhodopsin photointermediates are not sufficient to alter the globally fitted time constants. Consequently, the data for all sample types were fit simultaneously to produce the same set of apparent lifetimes (118 μs, 350 μs, and 1.5 ms), and their corresponding *b*-spectra were used to evaluate the kinetic scheme.

The absorbance changes (*b*-spectra) corresponding to each process for rho/bcp and rho samples and the fit of Scheme 1 to rho *b*-spectra are displayed in Figure 3. Comparison of *b*-spectra for each process in the 600 nm region between rho/bcp and rho reveals pH changes in the aqueous environment: positive absorbance in b_1 (the 118 μs process) and to a smaller degree in b_2 (the 350 μs process) indicate that the environment is becoming more acidic, whereas the substantial negative absorbance change near 600 nm in b_3 (the 1.5 ms process) indicates that the environment is becoming more basic. The positive absorbance in b_0 (the time-independent process) shows that a more alkaline medium prevails at the end of the reactions. Scheme 1 provides a good fit to rho *b*-spectra, in agreement with previous studies of late intermediate kinetics (*1, 7, 12*).

Separation of Rhodopsin and Dye Spectral Changes. Deviations of the dye kinetics from the rhodopsin time-dependent changes may not have been detected in the global

exponential fitting due to the relatively small amplitudes of dye absorption changes compared to the rhodopsin absorbance changes. Only after absorption changes due to rhodopsin kinetics have been removed from the data can the true kinetics of the dye signal containing only protonation information be determined. A natural way to account for the contribution of rhodopsin spectral changes in the experimental data recorded in the presence of dye is to use the absorption difference spectra of rhodopsin recorded in the absence of dye or in a well-buffered solution. In practice, however, this approach is not ideal because the variability of experimental data coming from different experiments is big enough to distort the spectral information carried by the dye. Also the efficiency of buffers in micellar systems may be different from that observed in solutions.

An alternative approach to determine the contribution of rhodopsin is to calculate it from the time-dependent concentrations of intermediates and their absorption spectra as determined directly from the rho/bcp sample. To obtain the microscopic rates and the time dependence of the intermediate concentrations, an iterative process was used. First rho/bcp *b*-spectra were fit to Scheme 1 using the intermediate spectra that gave the best fit to the rho data. As expected, the rho/bcp *b*-spectra could not be reproduced exactly by using rhodopsin intermediate spectra alone. The difference between the rho/bcp experimental *b*-spectra and the fit using only rhodopsin photointermediate spectra had the shape of the dye titration spectrum and was regarded as a first estimate for the dye spectral contribution. The amplitude of the dye contribution to each *b*-spectrum was determined by fitting the titration spectrum of the dye (Figure 1) to these "peeled-off" difference spectra. Next, the rho/bcp experimental *b*-spectra were corrected for the dye spectral contributions using the dye titration spectrum with the appropriate amplitudes.

The *b*-spectra thus corrected were very similar to the rho *b*-spectra and were fit to the kinetic scheme (Scheme 1) using the same intermediate spectra as before. In this second fitting procedure, the deviations between the *b*-spectra and the fit were much smaller and the second fit was able to more accurately represent the rhodopsin spectral changes because dye changes present during the first fit had been largely removed from the data. By using this second fit and the original rho/bcp experimental *b*-spectra, the "dye-peeling" procedure and *b*-spectra correction were repeated. This refinement continued until the corrected *b*-spectra showed no further changes and could be regarded as free of the dye spectral component. Figure 4a shows the rho/bcp *b*-spectra separated from dye spectral changes as well as the fit of Scheme 1 to these spectra. The microscopic rates obtained from the fit are similar to the corresponding ones for rho (see Table 1), indicating the success of the separation procedure.

The difference between the initial rho/bcp *b*-spectra and the last fit to the *b*-spectra produces *b*-spectra in which the rhodopsin kinetics have been removed, leaving behind proton signal *b*-spectra. Although the peeling-off procedure described above pulls all the experimental noise and errors into these spectra, their shape represents the dye titration curve reasonably well. The proton signal *b*-spectra could be extracted within a few cycles. These *b*-spectra and their model counterparts are shown in Figure 4b. The fact that

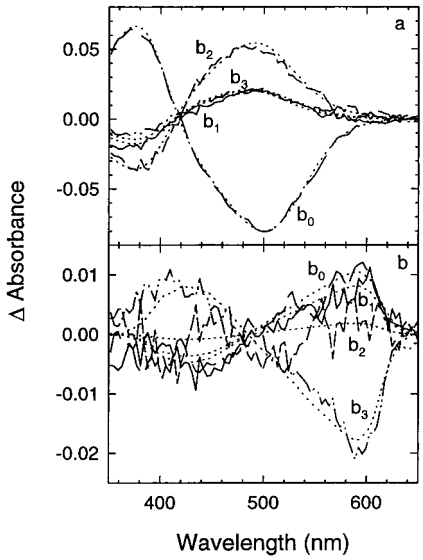

FIGURE 4: Separation as described in the text of rhodopsin and indicator dye contributions to *b*-spectra from Figure 3a. (a) *b*-Spectra of rhodopsin stripped of dye contributions and fit of Scheme 1. (b) *b*-Spectra of indicator dye and model *b*-spectra of proton signal. Line types are as follows: (—) for b_1, (---) for b_2, (—••—) for b_3, (— — —) for b_0, and (•••) for fit and model *b*-spectra.

Table 1: Microscopic Rates Corresponding to Fit of Scheme 1 to *b*-Spectra of Three Types of Purified Rhodopsin Samples Solubilized in Dodecyl Maltoside at 20 °C, pH 6.3[a]

sample type	rho (s^{-1})	rho/bcp, stripped (s^{-1})	rho/bcp/MES (s^{-1})
k_1	4300	3600	3700
k_2	1600	1600	1500
k_3	4900	5600	5600
k_4	470	560	470
k_5	690	690	690
k_6	~0	~0	~0

[a] Rhodopsin only (rho), rhodopsin with bromocresol purple (rho/bcp) stripped of dye, and rhodopsin with bromocresol purple and MES (rho/bcp/MES).

the proton signal *b*-spectra could be quickly extracted and have the shape of the dye titration curve provides evidence that the differences between rho and rho/bcp *b*-spectra are indeed due to dye protonation changes.

The time dependence of photointermediate concentrations was calculated from the kinetic matrix of Scheme 1 fitted to rho and rho/bcp *b*-spectra stripped of dye and appears in Figure 5. The product of the time-dependent intermediate concentrations and the intermediate spectra was subtracted from the rho/bcp absorption difference spectra leaving behind the spectral changes (and all the experimental noise) due to the proton response of the dye. The time-dependent amplitude of the dye signal is obtained by normalizing it to the dye titration curve shown in Figure 1 and is also shown in Figure 5. Since this dye signal represents only protonation changes it is not required to have the same kinetics as the rhodopsin absorption changes. However, within the signal-to-noise ratio of the data this signal was adequately fit with the same time constants as those that fit the rhodopsin photointermediates.

DISCUSSION

Proton Changes in rho/bcp Difference Spectra and b-Spectra. The decrease in the 600 nm region for the rho/bcp

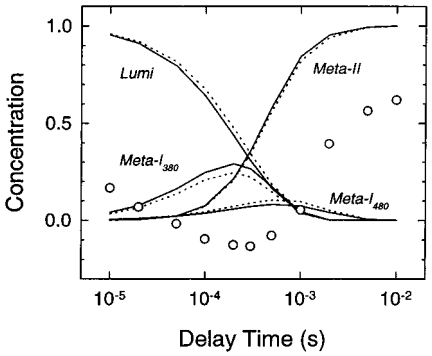

FIGURE 5: Time dependence of intermediate concentrations according to Scheme 1 for purified rhodopsin solubilized in dodecyl maltoside and net relative proton concentration changes reported by indicator dye (open circles) at 20 °C, pH 6.3. Line types are (—) for rhodopsin without dye and (···) for rhodopsin stripped of dye.

absorption difference spectra in the 10 μs to about 200 μs time interval after photolysis indicates that the environment is becoming more acidic, suggesting that rhodopsin is releasing protons into the aqueous medium during this time. The absorbance increase in this region between about 1 and 10 ms after photolysis indicates that the environment is becoming more basic, suggesting that rhodopsin is accepting protons from the aqueous medium during this later time frame (see Figure 2c).

Inspection of the rho/bcp *b*-spectra reveals more information regarding the processes involved in proton release and uptake (see Figure 3a). The eigenvectors of the kinetic matrix obtained by fitting rho *b*-spectra to Scheme 1 (see Figure 3b) reveal the composition of each *b*-spectrum: b_1 represents the decay of Lumi to Meta-I_{380}, b_2 represents the decay of the equilibrated mixture of Lumi and Meta-I_{380} to both Meta-I_{480} and Meta-II, and b_3 represents the decay of Meta-I_{480} to Meta-II. The time-independent b_0 is a difference spectrum between Meta-II and rhodopsin.

The positive *b*-spectral absorbance in the 600 nm region for the fast process (b_1) suggests that rhodopsin releases protons to the environment during the conversion of Lumi to Meta-I_{380}. The proton release seen by Arnis et al. (*17*) under conditions where proton uptake is suppressed (pH 8) is probably distinct from this early proton release since under those conditions Meta-I_{380} has decayed even at the earliest time studied. Because proton diffusion limits the time resolution of the indicator signal, it is not clear if intermediates earlier than Lumi are involved in the signals seen here. This possibility will be investigated in future studies.

The slight positive *b*-spectral absorbance in the 600 nm region for the middle process indicates that protons are released into the environment when Lumi decays to Meta-I_{480} and to Meta-II via Meta-I_{380}. The substantial negative *b*-spectral absorbance in this region for the slow process suggests that the protein accepts protons from the aqueous medium during the conversion of Meta-I_{480} to Meta-II. The observation of proton uptake between Meta-I_{480} and Meta-II is in agreement with previous studies near 4 °C in digitonin suspensions (*2, 18*).

The net protonation change during each process can be seen more clearly in the proton signal *b*-spectra (see Figure 4b). The proton signal *b*-spectra for the fast and slow processes have significant amplitudes, indicating that the

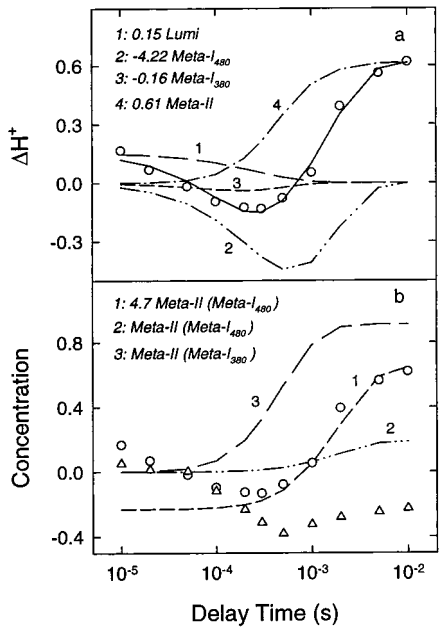

FIGURE 6: Assignments of protonation changes to intermediates of rhodopsin according to Scheme 1 to reproduce the time dependence of the net relative proton concentration change detected by bromocresol purple in solubilized rhodopsin at pH 6.3 and 20 °C. (a) Protonation changes of intermediates relative to rhodopsin (lines 1−4), the actual net protonation change measured by the indicator dye (open circles), and reproduced net change (solid line). (b) Comparison of the late phase of the actual dye signal (open circles) with the kinetics of Meta-II formation in the Meta-I_{380} (line 3) and Meta-I_{480} (line 2) reaction paths. For better visualization the amount of Meta-II formed from Meta-I_{480} (magnified by 4.7 and shifted) is also shown (line 1) together with the dye signal in the presence of 50 mM buffer (triangles).

major proton changes occur during the interconversion between Lumi and Meta-I_{380} (b_1) and the interconversion between Meta-I_{480} and Meta-II (b_3). The large positive amplitude in the 600 nm region for the time-independent process indicates net proton uptake during Meta-II formation.

Comparison of Dye Signal and Intermediate Time Courses. The intermediate time course plots for rho/bcp spectral data stripped of dye spectral contributions (see Figure 5) show that the dye signal is delayed relative to Meta-II formation. The time constant of the dye signal appears similar to that of Meta-I_{480} decay, suggesting that major proton changes occur as Meta-I_{480} decays to Meta-II (see below).

To gain further insight into the relationships between the dye signal and the intermediates, the proton changes for each intermediate were isolated. The time course of the proton changes for each intermediate was obtained by multiplying the intermediate concentration profiles by an appropriate amplitude factor indicative of the number of protons released or taken up compared to rhodopsin. The sum of the proton changes for the intermediates at each time delay reproduces the dye signal. The proton changes for the intermediates were determined by a least-squares fit to the time course of the dye signal.

The time course of the proton changes for each intermediate and the net proton change obtained after adding the proton changes at each time delay are shown in Figure 6a. For comparison, the actual dye signal is also shown. The most unusual feature of the plot is the contribution of Meta-I_{480}. Its coefficient for the fit to the dye signal time course

indicates that four to five protons would be released when it forms and should disappear when it decays if Scheme 1 is correct. This is surprising and cannot be easily reconciled with the known properties of this intermediate. In particular, it disagrees with the known pH dependence of the equilibrium between Meta-I_{480} and Meta-II (*7*) and the fact that the Schiff base deprotonates during the conversion of Meta-I_{480} to Meta-II (*2*, *6*). This anomaly arises because Meta-II appears in two phases, with the first phase preceding proton uptake, while Scheme 1 contains only one protonation state for Meta-II. To investigate the possibility that two protonation states of Meta-II are involved, it is useful to estimate how much Meta-II is formed by each path in Scheme 1. By integrating the rates of intermediate formation separately in each individual step, the amount of Meta-II produced can be divided into two pools and the kinetics of the proton signal can be related to these separate paths in the kinetic scheme.

The amounts of Meta-II formed from Meta-I_{380} and from Meta-I_{480} are shown in Figure 6b together with the dye signal. The dye signal in the presence of buffer is also shown. In the buffered sample the dye signal levels off when the buffer becomes effective, around the time Meta-I_{480} is formed. The buffer thus seems to have little effect on the early part of the dye signal. Dye molecules at the protein surface or inside the micelles are not easily accessed by buffer and may report fast protonation changes. Also, the partition of the dye between the bulk water phase and the micelles may slightly vary in the course of the rhodopsin photoconversion. Indeed, the fact that the proton signal for the buffered sample levels off below 0 is an indication that this latter effect is occurring to some degree. The observed increase in the concentration of the protonated form of the dye is likely to result from increased partitioning of the negatively charged bromocresol into micelles after some of the negative charge on those micelles is neutralized by Meta-II formation. The presence of this signal in the buffered sample is not significant for the conclusions drawn here concerning the late proton signal because it is small compared to the late proton signal in the unbuffered sample. However, the early proton signals are smaller and, because of the uncertainty of the effective time constant of buffering, we restrict our interpretation of the early events to qualitative conclusions.

Clearly the rise of the buffer-dependent part of the dye signal parallels the formation of Meta-II from Meta-I_{480}. To indicate this point more clearly, the amplitude of the late Meta-II concentration curve is enlarged by a factor of 4.7, and the resulting concentration curve is downshifted to match the level of the buffered dye signal in Figure 6b. Again, the number of protons taken up in the Meta-I_{480} to Meta-II step is four to five, which is not very plausible. This contradiction can be removed by assuming a spectrally silent transition leading from the early Meta-II form to a protonated late form, identical with the spectrally silent proton uptake proposed by Arnis and Hofmann (*4*). This latter silent process is assumed to proceed with a rate similar to that of the Meta-I_{480} to Meta-II transition for consistency with the observed proton kinetics.

These arguments suggest that two forms of Meta-II exist. Meta-II formed via proton uptake from the environment, the time course of which is reflected in the dye signal, can be identified with the previously characterized intermediate Meta-II_b. Meta-II that occurs prior to the dye signal, and will accept further protons from the environment will henceforth be referred to as Meta-II_a'. A prime is used to distinguish this intermediate from the MII_a originally proposed by Arnis and Hofmann (*4*) which probably represents a mixture of Meta-I_{380} and Meta-II_a'. As before, Meta-II will refer to the intermediate in Scheme 1 which represents the sum of the two isospectral forms. Although both forms of Meta-II have deprotonated Schiff bases (as indicated by their absorption spectra), only formation of Meta-II_b follows the dye signal.

Schemes Incorporating Two Forms of Meta-II. A recent time-resolved absorption study of the pH dependence of the late intermediates of rhodopsin in membrane also suggested that two forms of Meta-II, one deprotonated and one protonated, accounted for the observed kinetics. That study suggested that the kinetics are described by the following scheme (*7*)

Scheme 3

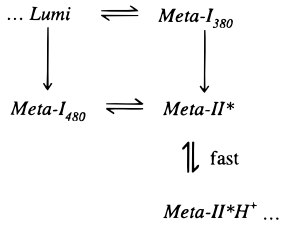

where Meta-II* and Meta-II*H^+ were presumed to exist in rapid equilibrium. In the detergent preparations studied here the fact that proton uptake is delayed relative to Meta-II formation shows that the equilibrium between Meta-II_a' and Meta-II_b is not fast compared to Meta-I_{480} decay. A mechanism like Scheme 3 can still be used to describe the detergent data if we assume that only three exponentials are observed because of degeneracy or near degeneracy of the Meta-I_{480} and Meta-II_a' decay rates. Since the decay of Meta-I_{480} parallels the rise of the dye signal (see Figure 6b), the estimates for the microscopic rates for the interconversion between Meta-II_a' and Meta-II_b were restricted to values whose sum equaled the third apparent rate obtained in the global exponential fitting. In Scheme 1, when a single Meta-II was used, the third apparent rate represented the sum of the microscopic rates for the interconversion between Meta-I_{480} and Meta-II. It was expected that the kinetic matrix of Scheme 3 under these restrictions would yield degenerate or quasi-degenerate solutions which would be in accord with three exponentials obtained in the global fit to the experimental absorption data. We therefore propose the following reaction scheme to describe rhodopsin bleaching in detergent:

Scheme 4

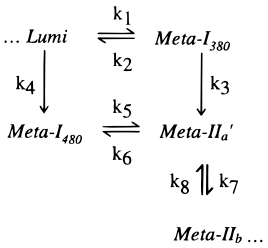

The microscopic rates obtained by fitting the data with Scheme 4 are shown in Table 2. The time courses of the

Table 2: The Microscopic Rates for Fits to Schemes 4 and 5 for Purified Rhodopsin Samples Solubilized in Dodecyl Maltoside at 20 °C, pH 6.3

scheme	Schemes 4 and 5 (s^{-1})
k_1	3640
k_2	1560
k_3	5550
k_4	556
k_5	691
k_6	<1
k_7	449
k_8	243

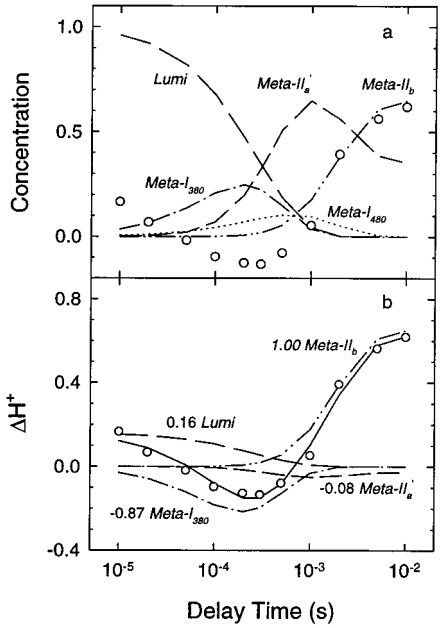

FIGURE 7: Time dependence of relative concentrations and protonation changes of rhodopsin intermediates according to Scheme 4. Intermediate concentrations and protonation numbers were determined from microscopic rates obtained by fitting Scheme 4 to *b*-spectra and lifetimes with the assumption of degeneracy of the kinetic matrix and whole number of proton uptake in the Meta-II$_a$′ → Meta-II$_b$ step. (a) Relative concentrations of rhodopsin intermediates according to Scheme 4. Open circles represent the net relative protonation change reported by the indicator dye. (b) Time course of protonation changes of intermediates relative to rhodopsin. Positive numbers refer to proton uptake, negative ones to proton release. The calculated (solid line) and experimental (open circles) net protonation changes are also shown. Because of temporal coincidence of Meta-I$_{480}$ and Meta-II$_a$′, and the relatively small amount of Meta-I$_{480}$ present, only protonation changes of Meta-II$_a$′ are considered.

concentrations of intermediates for the fit to Scheme 4 appear in Figure 7a. Also shown is the time course of the dye signal. The time course of Meta-II$_b$ formation parallels that for the dye signal, and the lifetime of Meta-II$_a$′ is similar to that of Meta-I$_{480}$. To gain insight into the relationship between the dye signal and the intermediates, once again the proton changes for each intermediate were calculated and their sum at each delay time was plotted and compared with the dye signal (see Figure 7b). The exact number of protons taken up by Meta-II$_b$ depends on the value chosen for the ratio of k_7 to k_8, which cannot be independently determined. For a completely forward-shifted equilibrium the value is slightly below 1 and the ratio k_7/k_8 used here has been chosen to make the number of protons taken up be 1. Because the concentration curves for Meta-I$_{480}$ and Meta-II$_a$′ coincide in time, protonation changes caused by these intermediates cannot be separated. Meta-I$_{480}$ is less likely to be involved in proton uptake or release than Meta-II$_a$′; therefore, we do not assign proton changes to the Meta-I$_{480}$ intermediate. The plots indicate that the major proton changes occur during the formation and decay of Meta-I$_{380}$ and the formation of Meta-II$_b$. Other schemes have been considered (see Appendix), but they are not as satisfactory as Scheme 4.

In the time-resolved absorption study of the pH dependence of the late intermediates in membrane suspensions (*7*), Scheme 3 was proposed to explain base catalysis associated with Meta-II formation. It was suggested that a rapid equilibrium between Meta-II* and Meta-II*H$^+$ accounted for the observation of only three exponentials for five intermediates. Analysis of the membrane data reveals that Scheme 4 predicts the correct trend for the pH dependence of the back reaction for the equilibrium between Meta-I$_{480}$ and Meta-II$_a$′, whereas Scheme 5 (see Appendix) predicts the opposite trend. Thus, a mechanism with the same connectivity as Scheme 4 is likely to describe the kinetics of rhodopsin late intermediates for both membrane and detergent suspensions of rhodopsin. Of course, it must be noted that kinetic analysis can disprove but not prove a given mechanism, and while Scheme 4 fits the data other more complex schemes are not precluded.

The existence of two forms of Meta-II was first proposed by Emrich and Reich (*19*). They suggested that the conformational change from Meta-I$_{480}$ to Meta-II involved the formation of a species that was spectroscopically observed before proton uptake. While that work needs to be interpreted carefully because samples were more impure than in later work and because of possible differences between membrane and detergent preparations, we can confirm the main conclusions presented there. The spectroscopically observed form would constitute a mixture of Meta-I$_{380}$ and Meta-II$_a$′, and the form occurring after proton uptake would be the equivalent of Meta-II$_b$. Similar behavior was seen by Baumann and Zeppenfeld (*20*) in their pH studies of the interconversions of metarhodopsins in sonicated frog rod outer segments. They also suggested a rapid equilibrium between two forms of Meta-II.

As mentioned in the Introduction, Arnis and Hofmann (*4*) have proposed the existence of two forms of Meta-II, called Meta-II$_a$ and Meta-II$_b$, where the formation of Meta-II$_b$ involves proton uptake from the aqueous environment. Photoregeneration from the signaling state (*5*) has then associated the proton uptake between Meta-II$_a$ and Meta-II$_b$ with the conformational change preceding transducin binding. Here, in addition to that change, we detect an earlier 380 nm absorbing intermediate displaying an early proton release reaction. It remains to be investigated whether, with the formation of Meta-I$_{380}$, the Schiff base proton leaves the protein. This would modify the suggestion from FTIR work that the Schiff base proton is translocated to its counterion, the carboxyl group of E113 (*21*), allowing counterion protonation from another protein group under some circumstances.

The time course of Meta-II$_b$ determined from the data presented here is somewhat different from what was observed in previous experiments. However, differences in observation method and analysis strategy could plausibly be responsible for this. Comparison of results from fundamen-

tally different strategies often leads to questions such as these. Consequently it is important to conduct definitive experiments under conditions where all distinct phenomena can be observed simultaneously. Here we have performed such experiments to show that two forms of Meta-II can be detected even when the other 380 nm absorbing form, Meta-I_{380}, has been accounted for.

APPENDIX

Since the present study shows proton uptake between Meta-I_{480} and Meta-II_b, and Meta-II_a' forms before Meta-II_b (see Figure 6b), the following scheme was also tested:

Scheme 5

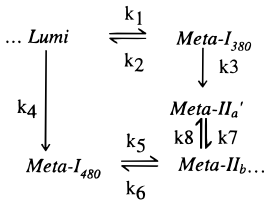

As with Scheme 4, the microscopic rates obtained by fitting the rho *b*-spectra to Scheme 1 were used. The microscopic rate for the transition from Meta-I_{380} to Meta-II in Scheme 1 was used for the transition from Meta-I_{380} to Meta-II_a' in Scheme 5, and the microscopic rate for the transition from Meta-I_{480} to Meta-II in Scheme 1 was used for the decay of Meta-II_a' as well as that of Meta-I_{480}. Scheme 5 also fits the data, indicating that a rapid equilibrium between Meta-II_a' and Meta-II_b (*7*) is not necessary. Its kinetic matrix also gives degenerate solutions. The microscopic rates are shown in Table 2.

Comparison of Models. Comparison of time courses reveals that both Scheme 4 and Scheme 5 predict approximately the same intermediate time courses. Also, a previously suggested scheme with equilibria between all intermediates (*1*) could be extended to fit these data. However, previous time-resolved absorption data for rhodopsin in sonicated disk membrane suspensions has indicated that one of the microscopic rates of the all equilibrium model appears to decrease with increasing temperature (*1*). While this process has a small amplitude, making this temperature dependence uncertain, this suggests that this model is less appropriate than Scheme 4 or Scheme 5. Further, we interpret the instability of the Simplex fitting method when applied to this model (*1*) as evidence that the all equilibrium model is an inadequate description of our data.

Scheme 4 and Scheme 5 represent two slightly different physical pictures of rhodopsin photoconversion. In Scheme 4 the branching from Lumi merges at Meta-II_a', and the last protonation step, believed to be a key step in receptor activation, is the same for all rhodopsin molecules. The changes, deprotonation of the Schiff base and, probably, proton uptake and conformational change of the protein leading from Lumi to Meta-II_a', occur in different order and manner in the two branches. In the Meta-I_{380} branch, deprotonation of the Schiff base and proton uptake by the protein are likely to occur in separate steps while in the Meta-I_{480} branch it seems to be a concerted step involving coupled intramolecular processes.

In Scheme 5, the two branches merge only at the final Meta-II_b intermediate. In the Meta-I_{380} branch the Schiff base deprotonation, proton uptake, and conformational changes are distributed among three consecutive elementary steps. In the Meta-I_{480} branch, the decay of Meta-I_{480} is likely to involve deprotonation of the Schiff base, uptake of two protons and, probably, a fair amount of conformational changes. This concerted step would require a good deal of cooperation between the different parts of the protein to accomplish of all these changes simultaneously. The molecular machinery of Scheme 4 thus seems to require less complexity than that required for Scheme 5.

REFERENCES

1. Thorgeirsson, T. E., Lewis, J. W., Wallace-Williams, S. E., and Kliger, D. S. (1993) *Biochemistry 32*, 13861−13872.
2. Matthews, R. G., Hubbard, R., Brown, P. K., and Wald, G. (1963) *J. Gen. Physiol. 47*, 215−240.
3. Emeis, D., Kühn, H., Reichert, J., and Hofmann, K. P. (1982) *FEBS Lett. 143*, 29−34.
4. Arnis, S., and Hofmann, K. P. (1993) *Proc. Natl. Acad. Sci. U.S.A. 90*, 7849−7853.
5. Arnis, S., and Hofmann, K. P. (1995) *Biochemistry 34*, 9333−9340.
6. Parkes, J. H., and Liebman, P. A. (1984) *Biochemistry 23*, 5054−5061.
7. Jäger, S., Szundi, I., Lewis, J. W., Mah, T. L., and Kliger, D. S. (1998) *Biochemistry 37*, 6998−7005.
8. Cohen, G. B., Yang, T., Robinson, P. R., and Oprian, D. D. (1993) *Biochemistry 32*, 6111−6115.
9. König, B., Welte, W., and Hofmann, K. P. (1989) *FEBS Lett. 257*, 163−166.
10. Lewis, J. W., Yee, G. G., and Kliger, D. S. (1987) *Rev. Sci. Instrum. 58*, 939−944.
11. Lewis, J. W., Warner, J., Einterz, C. M., and Kliger, D. S. (1987) *Rev. Sci. Instrum. 58*, 945−949.
12. Mah, T. L., Szundi, I., Lewis, J. W., Jäger, S., and Kliger, D. S. (1998) *Phochem. Photobiol.* (in press).
13. Hug, S. J., Lewis, J. W., Einterz, C. M., Thorgeirsson, T. E., and Kliger, D. S. (1990) *Biochemistry 29*, 1475−1485.
14. Henry, E. R., and Hofrichter, J. (1992) *Methods Enzymol. 210*, 129−193.
15. Goldbeck, R. A., and Kliger, D. S. (1993) *Methods Enzymol. 226*, 147−177.
16. Szundi, I., Lewis, J. W., and Kliger, D. S. (1997) *Biophys. J. 73*, 688−702.
17. Arnis, S., Fahmy, K., Hofmann, K. P., and Sakmar, T. P. (1994) *J. Biol. Chem. 269*, 23879−23881.
18. Ostroy, S., Erhardt, F., and Abrahamson, E. W. (1966) *Biochim. Biophys. Acta 112*, 265−277.
19. Emrich, H. M., and Reich, R. (1974) *Z. Naturforsch. 29c*, 577−591.
20. Baumann, C., and Zeppenfeld, W. (1981) *J. Physiol. 317*, 347−364.
21. Jäger, F., Fahmy K., Sakmar, T. P., and Siebert, F. (1994) *Biochemistry 33*, 10878−10882.

BI981249K